PCCP

Accepted Manuscript

This article can be cited before page numbers have been issued, to do this please use: D. Cibrev, M. Tallarida, C. Das, T. Lana-Villareal, D. Schmeißer and R. Gómez, *Phys. Chem. Chem. Phys.*, 2017, DOI: 10.1039/C7CP03958A.

ROYAL SOCIETY OF CHEMISTRY

rsc.li/pccp

New insights into water photooxidation on reductively pretreated hematite photoanodes.

Dejan Cibrev[a], Massimo Tallarida[b], Chittaranjan Das[b], Teresa Lana-Villarreal[a], Dieter Schmeisser[b], Roberto Gómez[a,*]

[a]Departament de Química Física i Institut Universitari d´Electroquímica, Universitat d´Alacant, Apartat 99, E-03080, Alicante, Spain.

[b]Applied Physics-Sensors, Brandenburg University of Technology, Konrad Wachsmann Allee, 17, 03046, Cottbus, Germany.

*Corresponding author: Email: Roberto.Gomez@ua.es

Abstract

It has been recently demonstrated that the photoactivity toward oxygen evolution of a number of n-type metal oxides can be substantially improved by a reductive electrochemical pretreatment. Such an enhancement has been primarily linked to the formation of low valent metal species that increase electrode conductivity. In this work, we report new insights into the electrochemical doping using highly ordered (110)-oriented hematite nanorods directly grown on FTO. The reductive pretreatment consists in applying negative potentials for a controlled period of time. Such a pretreatment was optimized in both potentiostatic and potentiodynamic regimes. We show that the optimized pretreatment enhances electrode conductivity due to an increase in charge carrier density. However, it additionally triggers changes in the morphologic, catalytic and electronic properties that facilitate the separation and collection of the photogenerated charge carriers causing an up to 8-fold enhancement in the photocurrent for water oxidation. The reductive pretreatment can be considered as a highly controllable electrochemical n-type doping with the amount of generated Fe^{2+}/polaron species and the change in film morphology as the main factors determining the final efficiency for water photooxidation of the resulting electrodes.

Keywords: hematite, doping, electrochemical pretreatment, water photooxidation, photoelectrochemistry.

1. Introduction

Hematite (α-Fe_2O_3) has recently emerged as a highly interesting photoanode material,[1] although its promising water splitting properties were already known almost four decades ago.[2] The renewed interest in hematite is based on: (i) a relatively small band gap of 2.1 eV which enables a significant light absorption of up to 40 % of solar radiation,[3] a (ii) valence band (VB) edge location that permits unassisted water photooxidation,[4] (iii) an excellent photo(electro)chemical stability in a broad pH range from 3 to 14[5] and (iv) an ample abundance as iron is the fourth most abundant element in the Earth's crust.[6]

In spite of these promising properties, the efficiency measured for water photooxidation, which is the rate determining step in water splitting, has been very low until recently. Such a limited behavior has been ascribed to the poor electron conducting properties of hematite as well as to a high degree of recombination (in the bulk and on the surface), as implicitly indicated by the extremely short lifetime of the photogenerated holes compared with other promising n-type semiconductors.[1] Recently, considerable effort has been devoted to surpass these drawbacks and to improve the efficiency for water oxidation. In this regard, nanostructuring,[7,8] surface modification[9,10] and particularly doping[11-14] have recently emerged as promising strategies.

One of the simplest and most direct ways to increase electron conductivity in hematite (and other n-type metal-oxide semiconductors) is reductive doping. The procedures that can lead to such a doping can be divided into two broad groups: (i) thermal annealing strategies conducted in reductive environments and (ii) reductive electrochemical pretreatments (in the dark or under illumination). The annealing procedures usually are synthetic steps. The oxide semiconductor is thermally treated in an oxygen deficient, an oxygen-free (nitrogen) or in a typical reductive (hydrogen) environment. This kind of treatment leads to a loss of stoichiometry and to the formation of oxygen deficient oxides. Such strategy has been vastly studied for TiO_2[15-20] and it has also been applied to α-Fe_2O_3.[21-23] Formally it has been interpreted as an introduction of Ti^{3+}/Fe^{2+} (or oxygen vacancies) in the crystal structure of the semiconductor, leading to an improved conductivity, a hindered electron-hole recombination, and an improved charge separation (band-bending). However, annealing, apart from being a costly procedure should be very precisely controlled as it can also lead to the deterioration of the

View Article Online
DOI: 10.1039/C7CP03958A

semiconductor intrinsic properties under non-optimized conditions. In this respect, the electrochemical reductive strategies offer distinctive advantages in comparison with the annealing procedures: (i) the electron doping process can be performed in-situ and (ii) it can be conducted in a very simple and highly controlled and reproducible fashion.[16,18] During the electrochemical pretreatment, electron accumulation occurs because of the application of a reductive potential/current program, which is accompanied by the consequent cation adsorption/intercalation process (for charge neutralization). Hence, structures with high internal surface area are especially suited for this kind of treatment.

Although the electrochemical doping strategies have become increasingly popular for TiO_2,[16,19,20] to the best of our knowledge, there only exists a previous study for Fe_2O_3, referring to a compact electrode of Ti-doped hematite, which is pretreated by applying negative potentials in the time domain of minutes.[24] A 4-fold improvement in the current for water oxidation under illumination at 0.23 V (vs. Ag/AgCl electrode) was measured. This enhancement was attributed to a reduction of the charge carrier recombination mainly as a result of a more efficient hole transfer to solution. Although, these results certainly suggest the potential of this doping strategy, such a reductive pretreatment drastically modified the electrode morphology, hindering an unequivocal conclusion.

In this work, we report for the first time the possibility of doping electrochemically nanostructured hematite electrodes based on nanorods. The optimized reductive pretreatment consists in applying a negative potential in the time domain of seconds. Upon this treatment, the photocurrent for water oxidation exhibits a six-fold enhancement. Apart from this practical optimization, we have performed an in depth physicochemical study, which unveils a complex picture. The electrochemical pretreatment induces changes in (i) the density of charge carriers (i.e. doping) (ii) the electrode morphology (iii) the surface hydroxylation (iv) the electrocatalytic properties and even (v) the electronic structure. All these factors determine the improvement in the photoelectrode performance toward water photooxidation.

View Article Online
DOI: 10.1039/C7CP03958A

2. Experimental

2.1 Synthesis of (110) oriented hematite nanorods

The employed synthesis is based on the work of Vayssieres and co-workers. It consists in a chemical bath deposition (CBD) followed by a thermal annealing.[25-27] Concretelly, 80 mL of an aqueous solution containing 0.15 mol·L^{-1} iron(III) chloride ($FeCl_3 \cdot 6H_2O$, Sigma-Aldrich, 99%) and 1 mol·L^{-1} sodium nitrate ($NaNO_3$, Panreac, 99%) were introduced into a regular screw cap flask containing FTO glass substrates supported with their conducting side against the flask wall. The flasks were heated in a regular oven at 100 ^{0}C for 6 h. The as-grown yellow FeOOH thin films were thoroughly washed with water and sonicated in an ultrasonic bath for 10 minutes to remove any residues from the synthesis. Finally, the electrodes were annealed in air at 600 ^{0}C for 1 h to induce the transformation of FeOOH into α-Fe_2O_3. The as-prepared hematite electrodes were transparent, with a homogeneous red coloration. The average thickness was 400 nm as measured using an Alpha Step D-100 profilometer.

2.2 Hematite film structural and morphological characterization

The crystal structure of hematite was identified by X-ray diffraction (Bruker D8-Advance, using Cu Kα radiation) with a rotatory anode operating at 40 kV and 40 mA. The morphological characterization of the hematite samples was conducted by SEM and TEM. SEM images were recorded with a Field Emission Scanning Electron Microscope, FE-SEM (Zeiss Merlin VP Compact) while TEM images were obtained with a Transmission Electron Microscope (JEOL JEM-2010). X-ray Photoelectron Spectroscopy (XPS) was used for the compositional analysis of the hematite surface (K-Alpha Thermo-Scientific).

2.3 Hematite (photo)electrochemical characterization

(Photo)electrochemical measurements were carried out in a standard three-electrode two-compartment electrochemical cell employing the hematite films as working electrodes and an Ag/AgCl/KCl (sat) electrode as a reference electrode (to which all the potentials are referred unless otherwise stated). A platinum wire was used as a counter electrode. The working electrolyte was a 1 mol·L^{-1} NaOH (Panreac, 98%) solution. The solution was purged with N_2 before and during the experiments. A scanning potentiostat (Potenciostat/Galvanostat AUTOLAB PGSTAT30) was used to record cyclic voltammograms in the dark and under illumination at a scan rate of 50 mV·s^{-1}. In addition, the electrochemical pretreatment, the potentiostatic photo-transients and the Mott-Schottky measurements were conducted using the same experimental set-up. A 1000 W ozone-free Xenon arc lamp (ORIEL Newport) was used for illumination. The

lamp irradiation was filtered through a water filter and a cut-off filter (Newport FSR-KG3 $\lambda \geq 350$ nm). The hematite electrodes were illuminated from the electrolyte side (EE). The incident light intensity was measured with a thermopile (Thorlabs PM100D) (power density of about 550 $mW \cdot cm^{-2}$). For the purpose of having comparable data, photo-transient measurements were also conducted with a standardized light intensity of 100 $mW \cdot cm^{-2}$ obtained by means of a AM 1.5 G solar simulator (Abet Technologies 2000).

2.4 Reductive electrochemical pretreatment

The reductive electrochemical pretreatment strategy consists in applying certain negative potentials (below -0.8 V) in the dark for controlled periods of time. After every pretreatment, the hematite electrode was brought to its steady state by applying a potential of 0 V until reaching a negligible current in the dark. After stabilization, the electrode photo-activity was tested by means of potentiostatic photo-transient measurements at 0.23 V, which corresponds to the reversible potential for oxygen evolution at the working pH. The studied reductive pretreatments were either potentiodynamic (cyclic) or potentiostatic in nature. Different negative potential limits in the range between -0.8 and -1.5 V were tested. In the potentiodynamic regime every single pretreatment consists in three cycles but only the third one is shown for each negative potential limit.. On the other hand, the potentiostatic pretreatments consist in applying a constant negative potential for 10 s. After this step, the procedure employed was the same as in the case of the dynamic pretreatment. In this respect, what we refer as the optimized pretreatment is the application of a potential of -1.3 V for 10 s. It is important to note that no visible color change in the hematite films was observed upon the electrochemical pretreatment unless the negative potential limit was -1.5 V, at which dark grey spots probably linked to the irreversible formation of FeO or other reduced species were observed.

2.5 Hematite spectroscopic characterization

The spectroscopic characterization of hematite was conducted to probe the electronic state distribution in the vicinity of the VB and conduction band (CB) edges by means of photoemission (PES) and X-ray absorption (XAS) spectroscopy, respectively. PES and XAS were measured using synchrotron radiation on the U49/2-PGM2 beam line at BESSY-II synchrotron radiation facility within the Helmholtz-Zentrum-Berlin. X-ray photons produced by the U49 undulator were monochromatized by a planar grating monochromator with a resolution of the order of $\Delta E/E \sim 10^{-4}$. XAS was measured using total electronic yield through the drain current on the sample. PES was measured using PHOIBOS-150 electron analyser from Spec GmbH, equipped with a 1D delay line detector. The base pressure of the measurement chamber was $5 \cdot 10^{-10}$ mbar.

View Article Online
DOI: 10.1039/C7CP03958A

3. Results

In this section, the morphological, structural and electrochemical characterization of the as-prepared hematite films will be presented first. Then, the electrochemical pretreatment will be introduced and its direct effect on the photocurrent magnitude for oxygen evolution will be shown. Finally, the morphological, compositional and electronic structure changes triggered by such a pretreatment will be presented.

As shown in Figure 1, the as-prepared hematite films display a homogeneous structure (Figure 1a) constituted by nanorods with a diameter in the range of 30 – 40 nm (Figure 1b). In some cases, such nanorods seem to be single crystals (Figure 1c) while in other cases they look like nanowire bundles (Figure 1b). The TEM images also reveal the crystalline nature of such nanorods (Figure 1c), which is confirmed by the XRD pattern (Figure 1d). Note that the majority of peaks in the diffractogram (see the black curve in Figure 1d) correspond to the crystalline FTO substrate. However, two additional peaks corresponding to hematite (See red pattern, Figure 1d) and associated with the (110) and (300) planes are also observed. This is in line with the anisotropic character of this highly oriented nanostructure.

The electrochemical experiments with these hematite films were conducted in alkaline media (pH = 13.6), due to their high chemical stability at this pH. Figure 1e shows the corresponding cyclic voltammograms in the dark and under illumination. Two important reference values ascribed to the equilibrium potentials for water reduction and oxidation have also been indicated. As shown in Figure 1e (black curve), the electrochemical response in the dark of the as-prepared hematite films corresponds well to that expected for a low-conductivity n-type semiconductor film. It is interesting to note that these films are almost inactive in the positive potential region in the dark. Under illumination, the as-prepared films show a photocurrent with a characteristic voltammetric sigmoidal morphology, while the electrochemical response of the negative potential region is radically changed. An additional peak and enlarged currents are observed. These faradaic currents can be ascribed to the reduction of the oxygen previously generated during the experiment at positive potentials. It is important to note that although the as-prepared hematite films exhibit relatively low photoactivity for oxygen generation (the photocurrent is quite modest), they show one of the lowest

View Article Online
DOI: 10.1039/C7CP03958A

values of photo-onset (-0.53 V as obtained from potentiostatic photo-transient measurements).

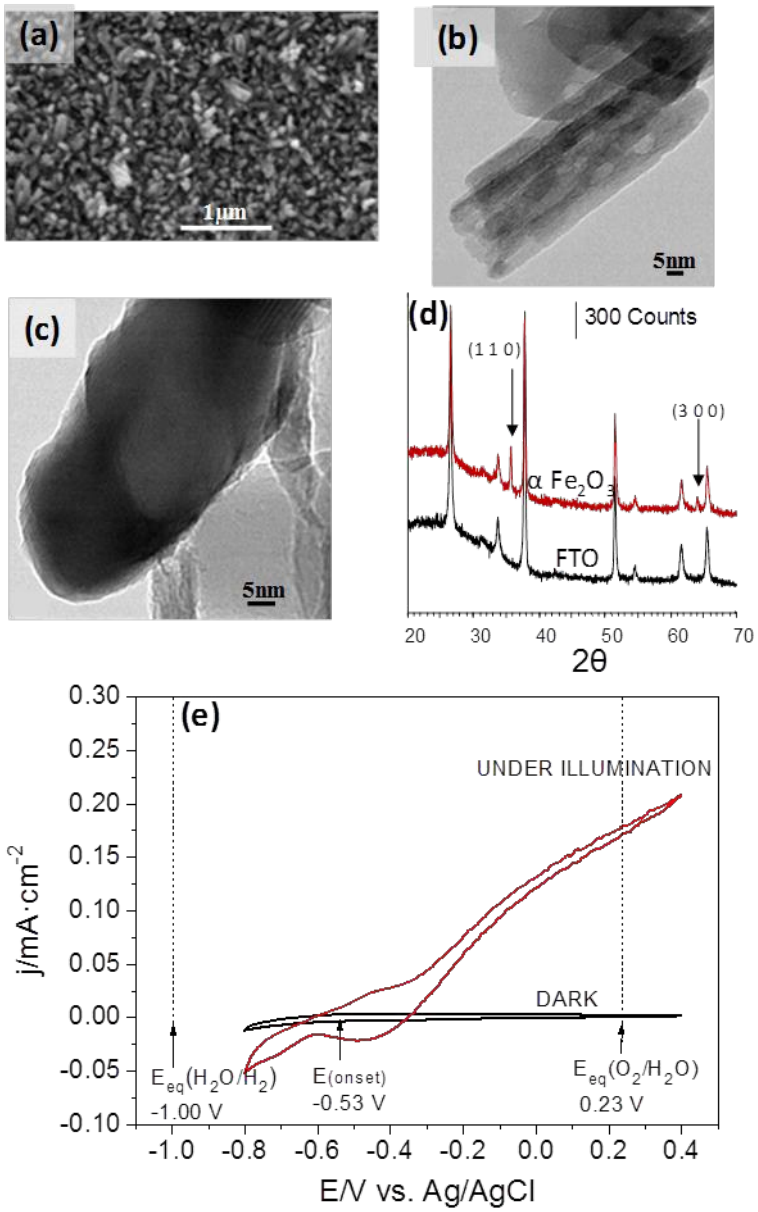

Fig. 1 a) SEM image of a hematite nanorod thin film grown on FTO; b) TEM image of a nanorod showing that it is constituted by nanowires; c) TEM image of a single crystal hematite nanorod; d) XRD pattern of hematite (red line) deposited on FTO (black line); e) Cyclic voltammograms for the as-prepared hematite nanorod electrodes in the dark (black curve) and under illumination (red curve). The reversible potentials for water reduction and oxidation as well as the hematite film photo-onset for oxygen evolution are marked with arrows.

Despite the promising morphological properties of the as-prepared hematite nanorods, the low photocurrents evince that a strategy is necessary to enhance such a low photoactivity. For this purpose, we have performed a reductive cyclic potentiodynamic pretreatment of the electrodes as shown in Figure 2a. The procedure is based on

applying 3 cycles from 0 V up to different negative potential limits in the range between -0.8 and -1.5 V, prior to measuring a photo-transient at 0.23 V (Figure 2b). As shown in Figure 2a, even for the less negative potential limit being used (-0.8 V), a small pseudocapacitive current (light brown curve) can be already seen, which increases significantly with decreasing the potential limit down to -1.1 V, at which symmetric capacitive signals are clearly observed (green curve). This is the expected behavior for a nanostructured n-type semiconductor.[28] At negative potentials, an accumulation region is usually observed due to electron accumulation accompanied by cation adsorption/insertion. Interestingly, when the negative potential limit is -1.2 V or more negative, an additional small oxidative peak appears at around -0.7 V which is located in the depletion region (Figure 2a, dark blue curve). For a compact Fe_2O_3 film in 1 M of NaOH, the $Fe^{3+} \rightarrow Fe^{2+}$ reduction has been reported to occur at -1.25 V (vs. Ag/AgCl/KCl).[29] Hence, a partial chemical reduction of hematite nanorod film is expected for pretreatments involving potential limits more negative than -1.2 V. Figure 2b shows the photocurrent transients for water oxidation after each pretreatment cycle. It is important to mention that after each pretreatment the electrodes were polarized at 0V until reaching a negligible dark current. The pretreatment clearly influences the shape and the magnitude of the photocurrent transients. In terms of magnitude, the photocurrent increases. In fact, the stationary photocurrent for oxygen generation is already doubled when the potential of the pretreatment is lowered from -0.8 to -1.1 V. In terms of shape, the photocurrent spikes significantly diminish as the potential limit lowers from -0.8 V down to -1.3 V. When the potential limit is -1.3 V, the photocurrent reaches a maximum value, being more than three times the initial one (Figure 2b, light blue curve). Lowering further the potential limit is not beneficial for the photo-activity of the hematite electrodes (Figure 2b, pink curve).

View Article Online
DOI: 10.1039/C7CP03958A

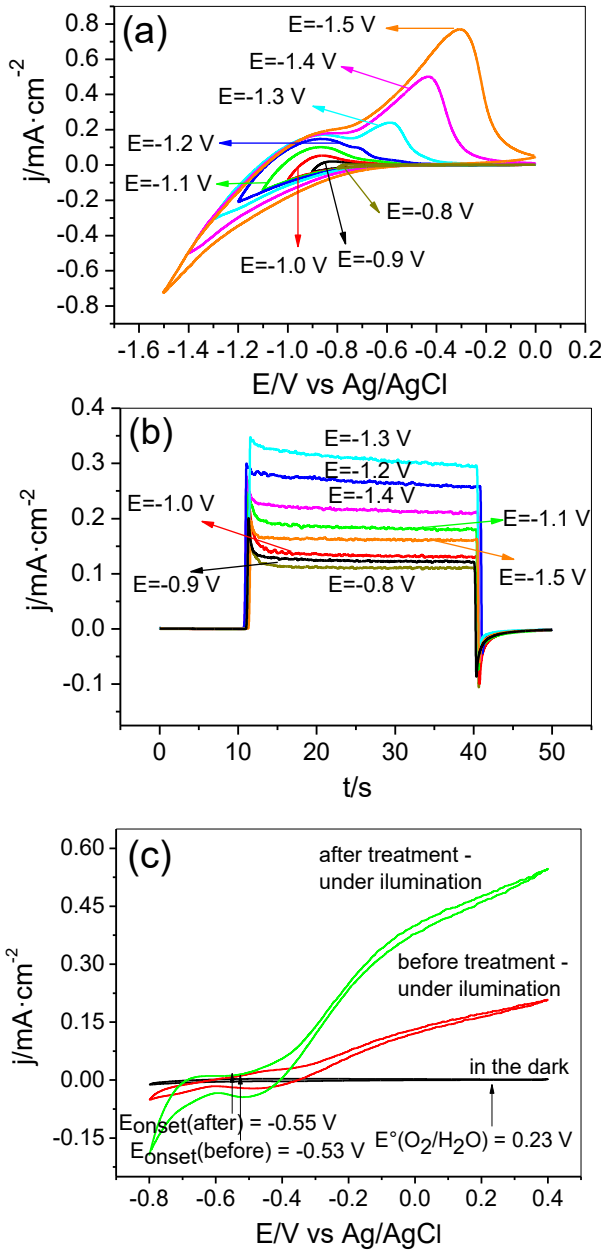

Fig 2. a) Cyclic voltammograms in the dark using different negative potential limits at a scan rate of 50 mV/s and b) the corresponding potentiostatic photo-transients at 0.23 V for nanorod hematite electrodes. The phototransient of the as-prepared electrode coincides with that of the electrode pretreated at -0.8 V and it is omitted for clarity c) Cyclic voltammograms in the dark (black curve) and under illumination before (red curve) and after (green curve) an optimized reductive pretreatment consisting in the application of 3 voltammetric cycles between 0 and -1.3 V at 50 mV/s.

As shown in Figure 2c, the voltammogram under illumination for the electrochemically optimized electrode (that treated down to -1.3 V, green curve) shows a remarkable improvement not only in terms of photocurrent magnitude, but also in terms of the

shape, ie. the slope of the photocurrent vs. potential curve is higher. Moreover, the photo-onset is shifted toward more negative values by 20 mV (see the arrows in the Figure 2c) with respect to the non-pretreated electrode.

In the aforementioned experiments the reductive pretreatment was dynamic and cyclic in nature. The notion that this strategy significantly improves the PEC properties of hematite boosted our interest toward an optimization of the pretreatment. In this regard, we also tested reductive potentiostatic pretreatments, in which the corresponding potential was applied for only 10 seconds. As shown in Figure 3, the potentiostatic reductive pretreatments also induce an enhancement of the water photooxidation process. Importantly, the photocurrent improvement is large, exhibiting a 6-fold increase in the case of the pretreatment at -1.3 V. As expected, the potentiostatic procedure is thus acting in a way similar to the potentiodynamic method, but inducing a larger change in the photocurrent when the potential is stepped to -1.3 V. As in the case of the potentiodynamic pretreatment, applying a potential below -1.3 V leads to a decrease in the resulting photocurrent.

Potentiostatic photo-transient measurements were also conducted with a standardized light intensity of 100 mW·cm^{-2} obtained by means of a solar simulator (AM 1.5, Figure S1). The conclusions are the same in qualitative terms: the optimized electrode pretreated at -1.3 V for 10 s shows an 8-times larger photocurrent than the as-prepared one (Figure S1, light blue curve).

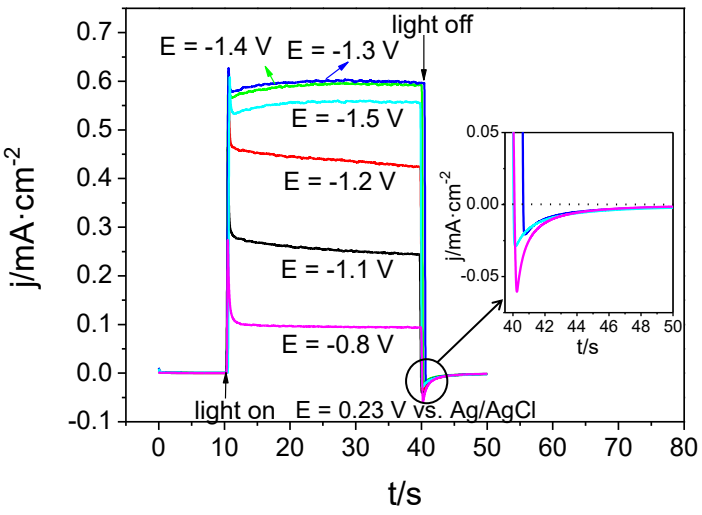

Fig. 3 Potentiostatic photo-transients at 0.23 V vs. Ag/AgCl/KCl for nanorod hematite electrodes in 1 M NaOH. Inset: photo-transient detail after turning off illumination (for the sake of clarity, only the curves for the -0.8 V, -1.3 V and -1.5 V pretreatment potentials are shown).

View Article Online
DOI: 10.1039/C7CP03958A

In the following, the electrochemical pretreatment was further refined using photocurrent transients as a test of photoactivity toward water oxidation. In this case, the pretreatment negative potential was fixed and applied for 10 s several times. Figure 4 shows the corresponding potentiostatic photo-transients upon each step. The photocurrent is clearly affected by the number of potential steps applied. However, the larger multiplication of the photocurrent occurs again when the electrode is biased at -1.3 V.

As shown in Figure S2, the first step already induces a 6-fold enhancement in the photocurrent. After 14 successive steps, the photoanode reaches its best performance, with an 8-fold improvement that declines on applying further steps. It is interesting to note that a continuous step for 140 s at -1.3 V leads to a significant deterioration of the electrode photo-activity (Figure S2B), which illustrates the fact that the reductive pretreatment is extremely sensitive to the way in which it is performed.

View Article Online
DOI: 10.1039/C7CP03958A

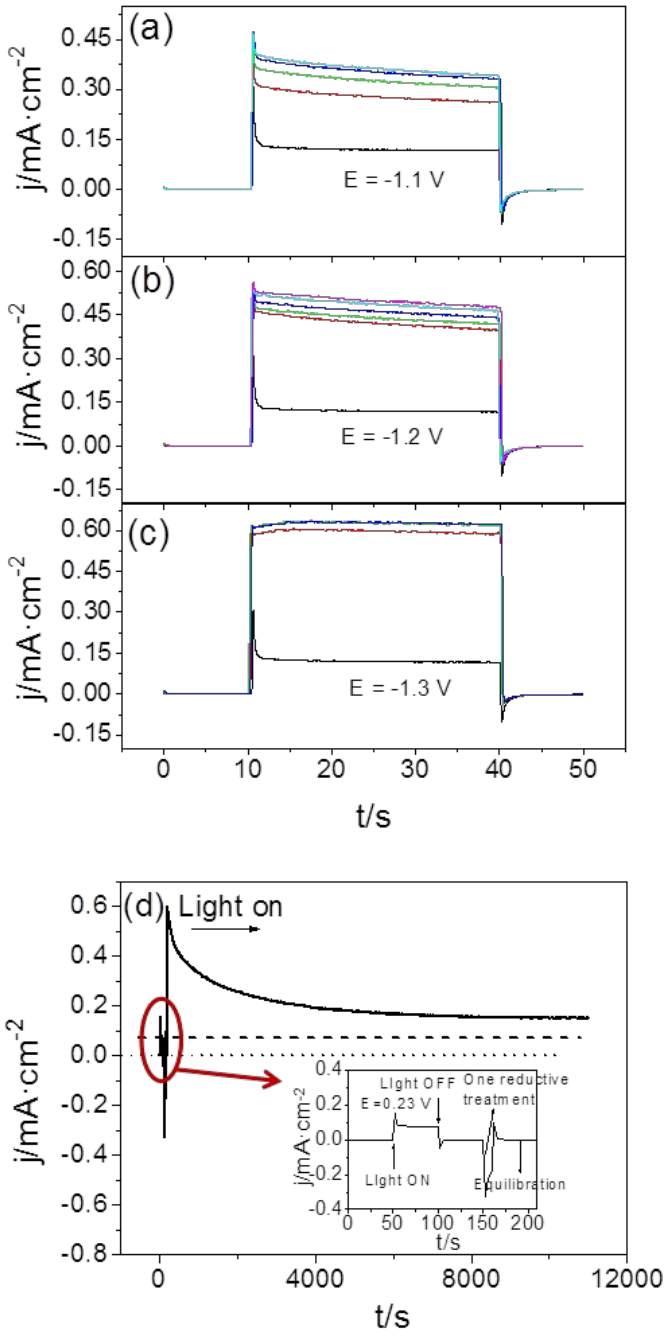

Fig. 4 Series of potentiostatic photo-transients conducted at 0.23 V after a pretreatment consisting in applying potentiostatic steps for 10 seconds at a) -1.1 b) -1.2 and c) -1.3 V vs. Ag/AgCl/KCl. d) Photocurrent evolution ascribed to water photooxidation measured at 0.23 V vs. Ag/AgCl/KCl for a hematite nanorod electrode tested under prolonged illumination (550 $mW \cdot cm^{-2}$) before (dashed line) and after (solid continuous line) one reductive pretreatment step at -1.3 V for 10 s in 1 M NaOH. Inset: Detail of the PEC characterization for the as-prepared electrode together with the reductive pretreatment.

The durability of the improvement caused by the reductive pretreatment was studied under potentiostatic conditions. This is critical to estimate the practicality of such a pretreatment as an ideal modification procedure should be permanent. The pretreated

View Article Online
DOI: 10.1039/C7CP03958A

electrode was kept at 0.23 V for more than 3 hours under continuous illumination. As shown in Figure 4d, after applying only one pretreatment step, a drastic improvement of the photocurrent for water oxidation occurs, which initially declines relatively quickly with time, reaching a quasi-stationary value that is still more than twice the initial value after three hours. This means that the reductive pretreatment is partially reversible. In any case, it is clear that the pretreatment involves long-term changes that are beneficial for the electrode efficiency. The strong oxidant conditions existent under strong illumination at sufficiently high potentials may provoke the partial reversion of the reductive pretreatment. This would of course contribute to a photocurrent decrease over time. It is worth noting that hematite is stable in the time scale of hours and thus the decay observed in fig. 4d should not be attributed to an intrinsic instability of the electrode material.

According to previous works,[15,30] an adequate electrochemical reductive pretreatment of n-type semiconductors induces an increase in the density of charge carriers, i.e. the electrode becomes doped. In order to investigate if this is the only reason for the photocurrent enhancement, we have performed a detailed study of the hematite electrodes after the electrochemical pretreatment, including the possible changes in the morphology. From a SEM analysis (see Figure S3), one may conclude that the pretreatment does not trigger significant changes of the electrode morphology, although the nanorod structure after the reductive pretreatment is slightly more dispersed than the densely packed original one. In any case, remarkable differences are discernible in the TEM images on a nanoscopic scale. As shown in Figure 5, which can be considered as representative of the whole sample, the reductive pretreatment induces the separation of the individual nanowires gathered in one nanorod. This change in the nanostructure is probably linked to the extensive adsorption/insertion of both sodium ions and protons that should take place to counterbalance the accumulation of electrons in the electrode. The resulting nanowire structure could contribute favorably to the photocurrent generation, as their diameter is less than 5 nm and the hole diffusion length in hematite is about 2-4 nm. Thus after the pretreatment, the path that holes have to cross to reach the solution would be reduced, resulting in a faster hole transfer to solution and a hindered electron-hole recombination.

This optimized structure composed of individuated nanowires possesses a higher contact area with the surrounding electrolyte in agreement with the enhanced

accumulation region observed in the cyclic voltammograms in the dark (Figure 5.c). Such an increment in the accumulation area of the pretreated films could also be an indication of a higher charge density of the pretreated films. In this regard, the Mott-Schottky plot (inset Figure 5.c) shows a smaller slope after the electrochemical pretreatment. This indicates that the reductive pretreatment triggers n-type doping to a certain extent. Specifically, the charge carrier density increases from 6.3 $\cdot 10^{19}$ cm^{-3} before up to 8.8 $\cdot 10^{19}$ cm^{-3} after the pretreatment. These values are in good agreement with similar calculations of charge carrier density on hematite nanorod electrodes taking into account only the geometric area of the electrodes.[31] However, it is important to note that the use of an uncorrected Mott-Schottky equation can lead to significant errors of the charge carrier density. In this regard, some of us have recently calculated more accurately the charge carrier density for nanorod films by using a corrected Mott-Schottky equation that takes into the account the real surface area (Eq. (1)) [32].

$$\frac{A_{real}^2}{C_{cs}^2} = \frac{2}{e\varepsilon\varepsilon_o N_d}\left(E - E_{fb} - \frac{kT}{e}\right) \quad (1)$$

where C_{cs} is the capacitance of the space charge region, A_{real} the real surface area, which takes into account the electrode roughness, e the elementary charge, ε the semiconductor dielectric constant, ε_o the vacuum permittivity, k the Boltzmann constant, T the absolute temperature, N_d the donor density, E the applied potential, and E_{fb} is the flat band potential. The ratio between the real and the geometric (projected) surface area defines the so-called surface roughness factor (r, Eq. (2)).

$$r = \frac{A_{real}}{A_{geom}} \quad (2)$$

If the real surface area is expressed through the surface roughness factor, an elegant version of the corrected Mott-Schottky equation can be obtained (Eq. (3)) that evinces that the slope is affected by this factor:

$$\frac{A_{geom}^2}{C_{sc}^2} = \frac{2}{e\varepsilon\varepsilon_o N_d r^2}\left(E - E_{fb} - \frac{kT}{e}\right) \quad (3)$$

In the case of a nanorod electrode the roughness factor can be obtained by (Eq. (4)):

$$r = 1 + 2\pi R h N_{col} \quad (4)$$

where R is the average nanorod radius, h the average nanorod height and N_{col} is the average density of nanorods per cm^2. Remarkably, introducing a roughness factor of 10.2, the corrected charge carrier densities are $6.0 \cdot 10^{17}$ cm^{-3} and $8.4 \cdot 10^{17}$ cm^{-3} respectively, differing in two orders of magnitude with respect to the case when only the geometric area is considered. We have considered that the roughness factor does not vary in a significant way upon the electrochemical pretreatment in spite of the changes reported above from TEM images. In any case, the conclusion of an enhanced charge carrier density after the reductive pretreatment seems to be valid.

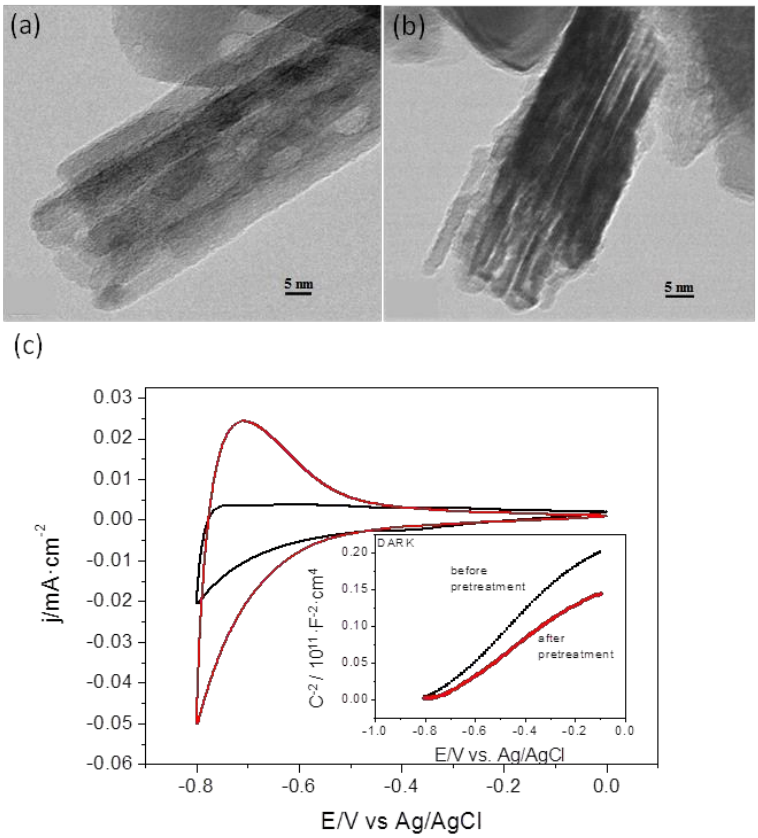

Fig. 5 TEM images for a nanorod before a) and after b) the electrochemical pretreatment, showing more clearly the individual nanowires. c) Cyclic voltammograms in the dark before (black curve) and after (red curve) the reductive pretreatment for hematite nanorod electrodes in 1 M NaOH. Scan rate: 50 $mV \cdot s^{-1}$. Inset: Mott-Schottky plots before and after the reductive pretreatment for hematite nanorod films obtained in the dark with a frequency of 1 kHz (perturbation amplitude of 5 mV). The pretreatment consisted in one step at -1.3 V for 10 s.

As long as the electrochemical pretreatment employs negative enough potentials as to reduce iron (III) to iron (II), the observed n-type doping may be related to the presence of Fe (II) in the pretreated films. To track the presence of Fe^{2+} in such films, hematite nanorods were analyzed by XPS. The Fe 2p spectra before and after the pretreatment

are virtually the same (see Figure S4) showing a typical satellite at binding energies of 719 eV, which is characteristic of Fe^{3+}.[33,34] Interestingly, no shoulder close to the Fe $2p_{3/2}$ peak indicative of the presence of Fe^{2+} was detected after the pretreatment.[35] These results could be justified by the extremely small amount of Fe^{2+} generated upon the electrochemical pretreatment which is probably below the detection limit of this technique, particularly bearing in mind that the pretreatment is always followed by an equilibration process conducted at 0 V until a negligible current in the dark is recorded. Admittedly we cannot completely discard an effect of exposing the sample to air during its transfer from the electrochemical cell to the XPS spectrometer.

The XPS of O 1s (Figure S5) also show typical spectral features for hematite with a peak at around 530 eV accompanied by a shoulder at higher energy values attributed to contributions of adsorbed water and hydroxyl ions. The analysis of these contributions indicates a slightly increased hydroxylation after the pretreatment.[36,37] In any case, the XPS of O 1s excludes the formal existence of FeOOH as a surface material because the ratio of the peak area $Fe\text{-}O^{2-}/Fe\text{-}OH^{-}$ is much lower than one[38] and it points to the presence of an overlayer of hydroxyl ions in the pretreated films.

To investigate the effect of the pretreatment on the dark oxygen evolution reaction, linear sweep voltammograms before and after the reductive pretreatment (in the positive potential region where this reaction occurs) were obtained. It is worth noting that from an electrochemical point of view, this reaction in the dark can be treated as an indicator of the ease of hole transfer to solution. It should also be borne in mind that the hematite electrode is not expected to follow a simple band edge pinning behaviour, thus allowing for the observation of an electrochemical behavior more akin to that of metals. At sufficiently positive potentials, holes are quickly consumed oxidizing hydroxide ions from the electrolyte and generating oxygen. As shown in Figure 6, the pretreated hematite shows a significantly improved electrocatalytic performance for oxygen evolution, not only in terms of current magnitude, but particularly in terms of onset potential. Specifically, the onset is shifted toward more negative potentials by 60 mV, while the Tafel slope before and after the pretreatment remains virtually unchanged, being 47 mV/dec as shown in the inset. This is a strong indication that the reaction mechanism for oxygen evolution remains unaltered, and that the improvement of the oxygen evolution reaction after the pretreatment is due to changes in either the kinetic constants or the physical properties of the solid. It has been proposed that the rate

View Article Online
DOI: 10.1039/C7CP03958A

determining step for oxygen evolution on hematite involves the generation of Fe^{IV} surface species.[39] The fact that the pretreatment is reductive is not directly related to the generation of Fe^{IV} species when a sufficiently positive potential is applied means that there is no contradiction between the nature of the treatment and the enhancement of the oxygen evolution reaction.

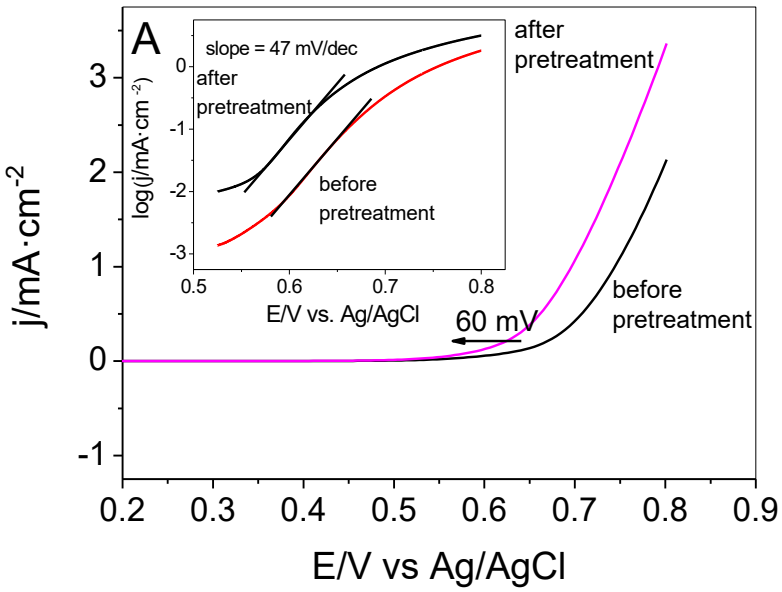

Fig. 6 Linear sweep voltammograms (5 $mV \cdot s^{-1}$) in the dark before and after the reductive pretreatment (one step at -1.3 V for 10 s) for a hematite nanorod electrode in 1 M NaOH. Inset: Tafel plots before and after the reductive pretreatment.

To investigate the changes in the electronic structure of the material after the pretreatment, the films were analyzed by emission and absorption spectroscopy coupled with a high intensity synchrotron radiation. XAS involves the excitation of electrons from a core state to an empty or partially empty state, providing information about the distribution of empty states in the CB. Figure 7.a shows the O 1s X-ray absorption spectra for (i) as-prepared (black curve), (ii) pretreated at -1.1 V (red curve) and (iii) for the (optimal) pretreated electrode at -1.3 V (light green curve). The main features of these spectra are a doublet of symmetric peaks at binding energies between 529 and 532 eV and a broad peak between 535 and 546 eV. The doublet can be attributed to the electronic transitions to anti-bonding O 2p states hybridized with 3d Fe states (t_{2g} and e_g orbital symmetry).[40,41] This doublet has been reported to be different for different iron oxides and its symmetric shape before and after the reductive pretreatment is considered as an indication of the hematite structure.[42] Moreover this notion together with the XPS

spectra is a strong indication that the electrochemical pretreatment is a soft modification strategy and does not trigger a phase transition of hematite. The broad peak at higher binding energies is generally attributed to transitions to anti-bonding O 2p states hybridized with iron 4s and 4p states.[40]

It is evident from Figure 7.a (light green curve) that the XAS spectrum of the optimized pretreated hematite is different from that of the non-optimized films, exhibiting a decrease in the doublet intensity accompanied with an increase in the broad peak located at higher binding energies. Interestingly, the electrode pretreated at -1.1 V (see the red curve) shows virtually the same spectral features as the non-pretreated hematite film, despite exhibiting almost double photocurrent. In any case, the slightly different spectral features for the electrode pretreated at -1.3 V (optimum pretreatment potential) indicate that its electronic structure has been modified as a result of the pretreatment. The decrease in the double peak intensity and the simultaneous increase of the broad peak intensity suggest a change in hybridization, which can be attributed to the generation of oxygen vacancies or formation of iron (II) species,[40] both triggered by potentials equal or more negative than -1.2 V.

To complete the analysis of the electronic structure modification triggered by the pretreatment, PES was conducted for hematite electrodes (i) pristine, (ii) pretreated at -1.1 V, and (iii) pretreated at -1.3 V. PES is a spectroscopic technique probing the occupied states by recording the number of emitted electrons. PES is thus complementary to XAS. PES and XAS allow to profile the electronic states in the VB and CB, respectively.

In Figure 7.b, the VB spectra for hematite samples are shown. They are characterized by two main features within the binding energy range of 0–10 eV. The broad peak at 4–9 eV has been assigned to mixed O 2p-Fe 3d and O 2p-Fe 4s4p contributions,[42] whereas the peak with a binding energy lower than 2.5 eV can be ascribed to polaron electron transfer or reduced iron species.[43] As shown in Figure 7.b, the spectra for pristine and -1.1 V pretreated hematite films show similar features in the low binding energy range, differing in the existence of one clear-cut peak between 11–12 eV, exclusively present in the case of the pristine film (see the black spectrum). Such a peak has no significant implications on the electronic structure as it is linked to chloride anions coming from

View Article Online
DOI: 10.1039/C7CP03958A

the film preparation.[44] In addition the -1.1 V pretreated sample shows a better-defined shoulder at 6-7.5 eV.

As in the case of XAS, the optimized film shows significant variations in its VB spectrum. The most striking feature is the contribution that develops at binding energies lower than 2.5 eV (see inset in Figure 7.b). The broad peak (see the light green curve) extending from 1 eV until 2.5 eV below the Fermi level considered as a reference energy can be related to (i) Fe^{2+} and (ii) polarons. In a recent study, some of us,[43] have distinguished between these two reduced species on the basis of two different contributions present in such a peak. In this case, the peak seems to also originate from these two contributions, that could have maxima at -1.4 and at -1.9 eV respectively, although an unambiguous distinction between them is not possible. In any case, it is evident that the optimized reductive pretreatment induces both polaron and Fe^{2+} formation. Therefore, it can be concluded that the electrochemical pretreatment at potentials more negative than -1.2 eV modifies the electronic configuration of hematite by introducing new electronic states also in the vicinity of the VB, which should affect its PEC properties for water oxidation.

View Article Online
DOI: 10.1039/C7CP03958A

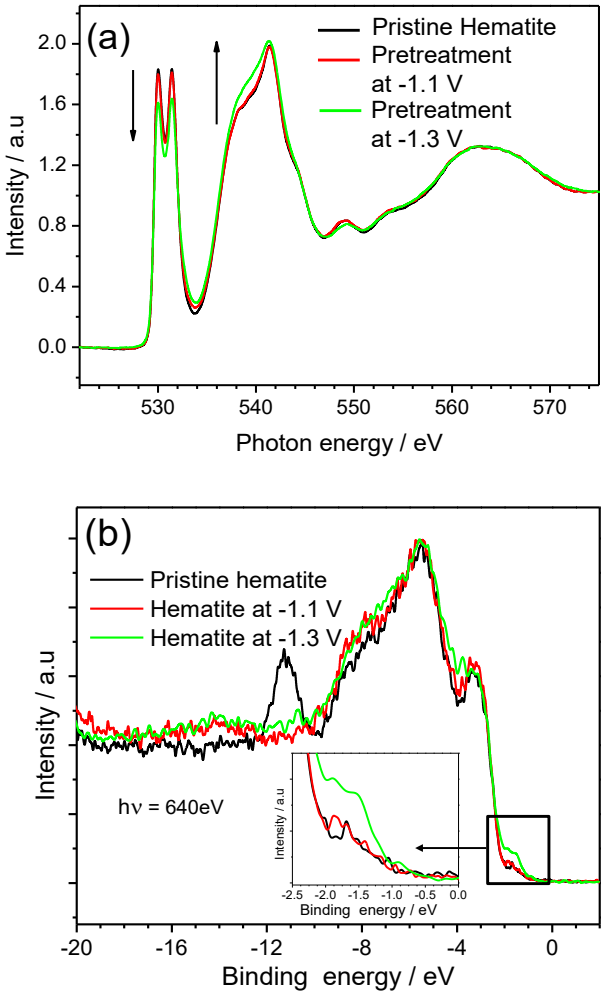

Fig. 7 a) X-ray absorption O 1s spectra for as-prepared (black curve), pretreated at -1.1 V for 10 s (red curve) and at -1.3 V for 10 s (light green curve) hematite nanorod electrodes. b) Valence band spectra recorded with excitation energy of 640 eV for hematite electrodes as-prepared (black curve), pretreated at -1.1 V (red curve) and pretreated at -1.3 V (light green curve). Inset: detail of the spectra in the low energy range.

4. Discussion

The recent advances in water photoxidation on hematite electrodes can be rationalized on the basis of a dual improvement model[¡Error! Marcador no definido.] that lies on the fact that hematite photoanodes suffer from both (i) a sluggish oxygen evolution kinetics, mostly affecting the photo-onset, and (ii) an unfavourable trade-off between a low absorption coefficient and a short hole diffusion length (resulting in a high degree of surface/bulk recombination) affecting mainly the photocurrent. With this picture in mind, the as-proposed enhancement strategies are based on: (i) introducing a passivating overlayer

View Article Online
DOI: 10.1039/C7CP03958A

and/or a good electrocatalyst on the electrode surface that facilitates hole transfer to solution, shifting the photocurrent onset; or (ii) a morphology control, i.e. the dimensions of the building blocks of the hematite structure can be optimized to favor electron transport to the back-contact, and hole transport to the semiconductor-electrolyte interface, increasing the photocurrent. This two-fold strategy does not consider in an explicit way that the control of the surface will also affect the photocurrent magnitude and that the morphology control, can also alter the photo-onset.

In this work we employ an improvement strategy based on applying a negative enough potential for a controlled period of time. Such a strategy has been previously described for other n-type semiconductors as a way to increase their charge carrier density. However, the present analysis shows that in the case of nanostructured hematite electrodes, this procedure induces additional changes in the morphology, and in the catalytic and electronic properties, which allows us to simultaneously address an improvement in the photo-onset (which is displaced by 20 mV toward lower values) and the photocurrent (which is multiplied by a factor of 8). Specifically, the optimized reductive electrochemical pretreatment is based on the application of a potential of -1.3 V vs. Ag/AgCl for a controlled period of time (in the range of seconds). This potential value fits within the potential window in which a compact hematite film is partially reduced.[29] In fact, when the pretreatment is performed in a cyclic potentiodynamic regime, an oxidative peak is observed that can be related to the back-oxidation process of $Fe^{2+} \rightarrow Fe^{3+}$. This anodic peak increases and shifts to more positive potentials as the negative potential limit becomes more negative. The potential shift can be related to the fact that, as the potential is scanned toward more negative values, the reduction of Fe(III) occurs at increasing depths within the film, demanding more positive potentials for the complete back-oxidation to occur and rendering the process less reversible. Importantly, apart from causing a partial reduction, the electrochemical pretreatment induces a loss of the structure compactness. This loss can be directly linked to the temporary formation of Fe^{2+} ions during the application of negative potentials. It is worth noting that, even if these species are not generated in large amounts, their larger size compared with Fe^{3+} can induce a significant stress in the structure that may trigger a change in the morphology individuating the nanowires that form the nanorods.

It is interesting to explore if there is a correlation between the electrocatalytic and the photoelectrocatalytic properties for water oxidation and their evolution with the

View Article Online
DOI: 10.1039/C7CP03958A

pretreatment potential. We have used as indicators of hematite electro- and photoelectro-catalytic activity, the oxygen evolution current at 0.8 V in the dark and the photocurrent at 0.23 V, respectively. As observed in Figure 8, the curve showing the electrocatalytic activity (Figure 8.a) is similar to that showing its photoelectrocatalytic activity (Figure 8.b) for water oxidation as a function of the pretreatment potential. Obviously, the enhancement of the photoactivity for water oxidation is intimately related with the corresponding improvement of the electrocatalytic behavior as the mechanism for oxygen evolution is expected to be the same except for the carrier generation. As mentioned, both curves follow similar trends with respect to the pretreatment potential, showing the largest activity for a pretreatment potential of -1.3 V.

As shown in Figure 8, when the pretreatment involves negative potential limits in the range from -1.2 to -1.3 V both the electrocatalytic activity and the photoactivity are simultaneously promoted. As deduced from the Mott-Schottky plots (see inset in Figure 5.c), the pretreatment at -1.3 V induces an increase in the charge carrier density, doping the film electrochemically. In addition, the spectroscopic characterization (see Figure 7) unveils new electron states, triggered by the pretreatment present in both the VB and CB. It should also be borne in mind that the pretreatment at -1.3 V induces a morphological change individuating the nanowires that constitute the nanorods.

Considering these factors one can explain the promotion of the electrocatalytic properties triggered by electrochemical doping. The increase in the charge carrier density should favor electron transport while the morphological change leads to an increase of the interfacial area. Both factors tend to increase the current for oxygen evolution. In addition, the pretreatment at -1.3 V seems to induce a minor hydroxylation of the surface (see Figure S5), which should improve slightly the reactivity toward oxygen evolution. All these factors can also favorably affect the photoactivity, i.e. the photocurrent. However, as it is evident from Figure 8, the maximum increase in the electrocatalytic activity is 60 %, while the photoactivity is multiplied by a factor of five. We can discard a faster charge carrier photogeneration rate upon electrochemical doping as a significant factor explaining the larger promotion of the photoelectrocatalysis compared to the electrocatalysis because no appreciable changes are observed in the UV-vis spectra after the pretreatment (see Figure S6). Therefore,

View Article Online
DOI: 10.1039/C7CP03958A

other factors apart from the enhanced conductivity and interfacial area (and hydroxylation) should contribute to determine the film photoactivity.

Photo-transient measurements can be used as a tool to obtain kinetic information on processes in which photogenerated charge carriers are involved. In this regard, the instantaneous peak current occurring when the light is switched on can be interpreted as a measurement of the initial flux of holes moving toward the surface.[45,46] The subsequent photocurrent decay until a steady state results from a gradual build-up of hole density in surface states, which induces recombination. The cathodic current observed when the light is switched off is due to recombination between electrons and the remaining long-lived holes trapped in surface states (see the detail in Figure 3). As shown in Figure 3, the on/off spikes are drastically diminished once the electrode is pretreated at -1.3 V. These results clearly evince that the pretreatment potential has a huge impact on electron-hole recombination in agreement with the observed photocurrent changes. Thus, the minimization of the electron recombination, due to the more favourable charge separation and transport triggered by the optimized pretreatment is clearly determining the hematite photoactivity.

At potentials more negative than -1.3 V, both the photoelectrocatalytic and the electrocatalytic activities diminish. We can expect that, as the pretreatment potential becomes more negative, an enhanced electron accumulation occurs. This should induce more drastic changes in the electronic structure. Specifically, additional states in the band gap might appear that can favor charge recombination[47] and lead to a decrease in the photocurrent. Note that recombination increases as the potential is being more negative than -1.3 V as revealed by the photo-transients. In addition, at such negative potentials, the nanowires suffer further unfavorable morphological alterations like rupture (Figure S7) and dissolution that should worsen the photoelectrochemical activity.

View Article Online
DOI: 10.1039/C7CP03958A

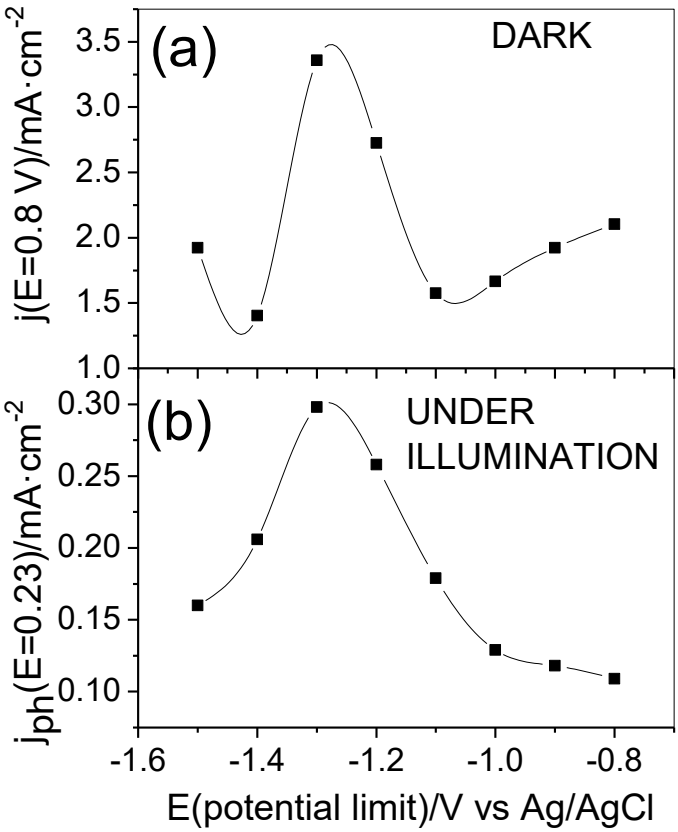

Fig. 8 a) Dark current density at 0.8 V and b) photocurrent density at 0.23 V vs Ag/AgCl/KCl (in 1M NaOH) for hematite nanorod electrodes previously pretreated at different potentials.

Admittedly, at pretreatment potentials less negative than -1.2 V, the electrocatalytic and the photoelectrocatalytic activity show opposing trends. While the former decreases, the latter increases upon lowering the pretreatment potential. As at these potentials the morphological and electronic alterations of the hematite nanostructure seem to be minor, surface related aspects should be crucial for explaining the trends. As observed in Figure 3, a pretreatment at -1.1 V triggers a significant change in the shape of the transients, indicating a reduced hole trapping and recombination. Such an effect would enhance the photoelectrocatalytic response without altering the electrocatalytic behavior in which carrier recombination is irrelevant.

In any case, these results confirm that some hematite intrinsic limitations such as a low conductivity and a fast carrier recombination can both be mitigated in-situ by a reductive electrochemical doping. This clearly demonstrates the potential applicability

View Article Online
DOI: 10.1039/C7CP03958A

of a precisely controlled electrochemical reductive pretreatment to promote water photooxidation on hematite nanorods.

5. Conclusions

Nanostructured (110)-oriented hematite nanorods prepared by means of chemical bath deposition on FTO conducting glass substrates were tested as photoanodes for water oxidation. Such nanorods show one of the lowest photo-onset values reported in the literature (-0.53 V vs. Ag/AgCl/KCl) for water oxidation. We have applied to these hematite electrodes a simple and highly controllable electrochemical pretreatment that entails the application of negative potentials for a time interval in the range of seconds. Such a pretreatment gives rise to an up-to eight-fold enhancement of the photocurrent and to a 20 mV negative shift of the photocurrent onset potential, triggering changes in electrode morphology, catalytic ability, and electronic structure. The morphological change consists in individuating the nanowires that form each nanorod. The reductive pretreatment enhances the density of charge carriers as revealed by Mott-Schottky measurements and induces new electronic states close to the CB and VB edges as confirmed by XAS and PES, respectively. The reductive pretreatment also provokes a significant slowdown of carrier recombination. Hence, electrochemical doping should not be considered simply as an n-type doping able to boost the photoactivity due to a better electron transport. Actually, our results clearly show that it induces more profound changes in the electronic structure and composition, which determine the final electrode electrocatalytic and photoelectrocatalytic activity. In fact, both properties follow a similar general trend with the pretreatment potential.

In a more general vein, the reductive pretreatment can be also applied to previously modified or doped hematite structures. In this regard, the synergetic effect of the reductive pretreatment on Ti-modified and Al-surface-modified hematite electrodes are underway in our laboratory. From a practical perspective, the electrochemical doping has the limitation of not being permanent, which means that it needs to be applied periodically. This is not a serious drawback in a practical device as long as the enhancement triggered by the pretreatment clearly offsets this limitation.

View Article Online
DOI: 10.1039/C7CP03958A

Conflicts of interest

There are no conflicts of interest to declare.

Acknowledgements

We are grateful to the Spanish MINECO for financial support through projects MAT2012-37676 and MAT2015-71727-R both supported with FEDER funds. D.C. is also grateful to MINECO for the award of an FPI grant.

Electronic Supplementary Information (ESI) available: [Transients under 1 sun illumination, effect of the number of pretreatment steps, effect of the pretreatment on SEM electrode images, XPS regions Fe 2p and O 1s, and UV-vis absorption spectra, TEM images on structural changes caused by hematite over-reduction]. See DOI: 10.1039/x0xx00000x

6. References

[1] K. Sivula, F. Le Formal and M. Grätzel, *ChemSusChem*, 2011, **2**, 432-449.

[2] K. L. Hardee and A. J Bard, *J. Electrochem. Soc.*, 1976, **23**, 1024-1026.

[3] L. A. Marusak, R. Messier and W. B. White, *J. Phys. Chem. Solids*, 1980, **41**, 981-984.

[4] J. E. Thorne, S. Li, C. Du, G. Qin and D. Wang, *J. Phys. Chem. Lett.*, 2015, **6**, 4083-4088.

[5] O. Zandi and T. W. Hamann, *Phys. Chem. Chem. Phys*., 2015, **17**, 22485-22503.

[6] P. C. K. Vesborg and T. F. Jaramillo, *RSC Adv*., 2012, **2**, 7933-7947.

[7] B. D. Alexander, P. J. Kulesza, L. Rutkowska, R. Solarska and J. Augustynski, *J. Mater. Chem*., 2008, **18**, 2298-2303.

[8] R. Van de Krol, Y. Q. Liang and J. Schoonman, *J. Mater. Chem.*, 2008, **18**, 2311-2320.

[9] Y. Zhang, Z. Zhou, C. Chen, Y. Che, H. Ji, W. Ma, J. Zhang, D. Song and J. Zhao, *ACS Appl. Mater. Interfaces*, 2014, **6**, 12844-12851.

[10] B. Klahr, S. Gimenez, F. Fabregat-Santiago, J. Bisquert and T. W. Hamann, *J. Am. Chem. Soc*., 2012, **134**, 16693-16700.

[11] J. A. Glasscock, P. R. F. Barnes, I. C. Plumb and N. Savvides, *J. Phys. Chem. C*, 2007, **111**, 16477-16488.

[12] N. T. Hahn and C. B. Mullins, *Chem. Mater.*, 2010, **22**, 6474-6482.

[13] Y. Ling, G. Wang, D. A. Wheeler, J. Z. Zhang and Y. Li, *Nano Lett.*, 2011, **11**, 2119-2125.

[14] T. –Y. Yang, H.-Y. Kang, U. Sim, Y.-J. Lee, J.-H. Lee, B. Koo, K. T. Nam and Y.-C. Joo, *Phys. Chem. Chem. Phys*., 2013, **15**, 2117-2124.

[15] H. Pelouchova, P. Janda, J. Weber and L. Kavan, *J. Electroanal. Chem.*, 2004, 566, 73-83.

[16] T. Berger, T. Lana-Villarreal, D. Monllor-Satoca and R. Gómez, *Electrochem. Commun.*, 2006, **8**, 1713-1718.

[17] B. H. Meekins and P. V. Kamat, *ACS Nano*, 2009, **3**, 3437-3446.

[18] D. Li, P.-C. Chang, C.-J. Chien and J. G. Lu, *Chem. Mater.*, 2010, **22**, 5707-5711.

[19] I. Idígoras, T. Berger and J. A. Anta, *J. Phys. Chem. C*, 2013, **117**, 1561-1570.

[20] A. Minguzzi, C. M. Sánchez-Sánchez, A. Gallo and V. Montiel, S. Rondinini, *ChemElectroChem*, 2014, **1**, 1415-1421.

[21] M. Forster, R. J. Potter, Y. Ling, Y. Yang, D. R. Klug, Y. Li and A. J. Cowan, *Chem. Sci.*, 2015, **6**, 4009-4016.

[22] Y. Ling, G. Wang, J. Reddy, C. Wang, J. Z. Zhang and Y. Li, *Angew. Chem. Int. Ed.*, 2012, **51**, 4074-4079.

[23] M. Li, J. Deng, A. Pu, P. Zhang, H. Zhang, J. Gao, Y. Hao, J. Zhong and X. Sun, *J. Mater. Chem. A*, 2014, **2**, 6727-6733.

[24] P. Shangguan, S. Tong, H. Li and W. Leng, *RSC Adv.*, 2013, **3**, 10163-10167.

[25] T. Lindgren, H. Wang, N. Beermann, L. Vayssieres, A. Hagfeldt and S.-E. Lindquist, *Sol. Energ. Mat. Sol. Cells*, 2002, **71**, 231-243.

[26] N. Beermann, L. Vayssieres, S.-E. Lindquist and A. Hagfeldt, *J. Electroanal. Chem.*, 2000, **147**, 2456-2461.

[27] L. Vayssieres, N. Beermann, S.-E. Lindquist and A. Hagfeldt, *Chem. Mater.*, 2001, **13**, 233-235.

[28] T. Berger, D. Monllor-Satoca, M. Jankulovska, T. Lana-Villarreal and R. Gómez, *ChemPhysChem*, 2012, **13**, 2824-2875.

[29] M. E. G. Lyons and M. P. Brandon, *Phys. Chem. Chem. Phys.*, 2009, **11**, 2203-2217.

[30] H. Cao, K. Huang, L. Wu, G. Hou, Y. Tang and G. Zheng, *Appl. Surf. Sci.*, 2016, **364**, 257-263.

[31] Y. Ling, G. Wang, D. A. Wheeler, J. Z. Zhang and Y. Li, *Nano Lett.*, 2011, **11**, 2119-2125.

[32] A. Cots, D. Cibrev, P. Bonete and R. Gómez, *ChemElectroChem*, 2017, **4**, 585–593.

[33] Z. Zhang, J. Lu, T. Yun, M. Zheng, J. Pan, C. H. Sow and E. S. Tok, *J. Phys. Chem. C*, 2013, **117**, 1509-1517.

[34] J. D. Desai, S. K. Pathan, S.-K. Min, K.-D. Jung and O. S. Jo, *Appl. Surf. Sci.*, 2005, **252**, 1870-1875.

[35] S. J. Roosendaal, B. van Asselen, J. W. Elsenaar, A. M. Vredenberg and F. H. P. M. Habraken, *Surf. Sci.*, 1999, **442**, 329-337.

[36] Y. Nie, C. Hu, L. Zhou and J. Qu, *Appl. Catal. B Environ.*, 2008, **82**, 151-156.

[37] T. Yamashita and P. Hayes, *Appl. Surf. Sci.*, 2008, **254**, 2441-2449.

[38] N. S. McIntyre and D. G. Zetaruk, *Anal. Chem.*, 1977, **49**, 1521-1529.

[39] T. Nakashima, K. Ishikawa and H. Irie, *Chem. Comm.*, 2016, **52**, 14015-14018.

[40] M. Li, J. Deng, A. Pu, P. Zhang, H. Zhang, J. Gao, Y. Hao, J. Zhong and X. Sun, *J. Mater. Chem., A* 2014, **2**, 6727-6733.

[41] J. Deng, X. Lv, J. Gao, A. Pu, M. Li, X. Sun and J. Zhong, *Energy Environ. Sci.*, 2013, **6**, 1965-1970.

[42] K. Gajda-Schrantz, S. Tymen, F. Boudoire, R. Toth, D. K. Bora, W. Calvet, M. Grätzel, E. C. Constable, A. Braun, *Phys. Chem. Chem. Phys.*, 2013, **15**, 1443-1451.

[43] M. Tallarida, C. Das, D. Cibrev, K. Kukli, A. Tamm, M. Ritala, T. Lana-Villarreal, R. Gómez, M. Leskelä and D. Schmeisser, *J. Phys. Chem. Lett*, 2014, **5**, 3582-3587.

[44] J. Stöhr, J. NEXAFS spectroscopy, Springer-Verlag, Heidelberg, Germany, **1996**.

[45] C. Y. Cummings, F. Marken, L. M. Peter, A. A. Tahir and K. G. U. Wijayantha, *Chem. Commun*, 2012, **48**, 2027-2029.

[46] S. M. Ahmed, J. Leduc and S. F. Haller, *J. Phys. Chem.*, 1988, **92**, 6655-6660.

[47] F. Le Formal, N. Tétreault, M. Cornuz, T. Moehl, M. Grätzel and K. Sivula, *Chem. Sci.* 2011, **2**, 737-743.

View Article Online
DOI: 10.1039/C7CP03958A

TABLE OF CONTENTS

Photoactivity enhancement of hematite nanorod electrodes upon a reductive pretreatment can be explained on the basis of morphological and electronic changes.